Numerical Modelling of Hydraulic Behaviour and Biogas Production from Paper Industry Effluents in an Anaerobic Digester

Abdelhay Laabyech[1,*], Samir Men-La-Yakhaf[1], and Fatima Kifani-Sahban[1]

ARTICLE INFO

Article history:
Received: 22 June 2023
Revised: 28 October 2023
Accepted: 25 January 2024
Online: 20 June 2024

Keywords:
Anaerobic digestion
Biogas production
Finite volume method
Hydrodynamics
Numerical model
Wastewater treatment plant

ABSTRACT

In this study, we focus on the anaerobic digestion of polluted effluents from the paper mill wastewater treatment plant (WWTP). More specifically, we examine biogas production and fluid hydraulic behaviour in the anaerobic digester. This paper presents a two-dimensional numerical modelling of fluid dynamics and biogas production. In this context, we present and detail the equations that describe this phenomenon: the conservative equations (mass, momentum and energy) solved by finite volume methods coupled to the Gauss-Seidel method for the compressible and incompressible cases and the system of biological equations of the degradation kinetics, representing the production of biogas, solved by the second order Runge-Kutta method. The main objective of this work is to understand the evolution of the physical and biological parameters of the anaerobic digestion process in the digester in order to improve biogas production. Thus, to know the impact of the gas produced on the characteristics of the fluid to simplify the complexity of similar studies. The numerical code developed met these expectations by providing results consistent with the data obtained experimentally by our team, while offering a satisfactory representation of biogas production at the Wastewater treatment plant. Our model has also enabled us to better understand the impact of the gas produced on the characteristics of the fluid inside the digester.

1. INTRODUCTION

During the various stages of the preparation and production process, pulp and paper mills use several chemical substances, as well as a considerable amount of water, ranging from 200 to 1000 m^3 per tonne of pulp [1, 2]. Consequently, they would discharge a huge volume of effluent laden with various highly contaminated pollutants, such as the organic matter constituting wood and substances such as resin acids, fatty acids, diterpenic alcohols and chlorinated resin acids [3, 4]. These effluents are harmful to the environment and must be treated using physical, chemical and biological processes prior to being discharged back into nature [5]–[7]. Among the biological treatments used for this type of effluent, anaerobic digestion has proved to be the most appropriate, duo to its notable depollution efficacy, capacity for greenhouse gas emission reduction, and energy efficiency [5, 8].

Anaerobic digestion involves various groups of micro-organisms break down complex organic matter into simple, stable end products [9]. These include biogas, primarily consisting of methane (CH_4) and carbon dioxide (CO_2), considered a renewable energy source, and solid residues known as digestate, which can be used as an organic fertiliser. Anaerobic digestion occurs in the absence of oxygen in biological reactors [10]–[12]. To ensure an efficient and optimal anaerobic digestion process in the digester, it is necessary to regulate several parameters. This ensures the creation of ideal conditions for the growth of micro-organisms and the smooth running of the anaerobic digestion stages. These are some of the essential parameters: temperature, pH, hydraulic retention time, organic load, carbon/nitrogen ratio and mixing [13]–[15]. Indeed, mixing plays a crucial role in anaerobic digestion. It maintains a uniform distribution of nutrients, temperature, pH and concentration in the digester. It promotes microbial interactions, optimising process efficiency and avoiding dead zones or areas of low activity. As a result, it improves biogas production [16, 17]. An adequate mixing speed is sufficient to ensure that the process runs smoothly while maintaining a balance between efficiency and energy consumption, unlike high or low mixing speeds. High mixing speeds promote good contact between the substrates in the digester, but have a negative effect on floc formation and lead to a reduction in biogas production. In addition, they lead to higher energy consumption. Low mixing speed allows good floc

[1]*Team of Modeling and Simulation of Mechanical and Energetic, Physical Department, Faculty of Sciences, Mohammed V University, 4 Av IBN BATTOUTA, B.P. 1014 RP, Rabat, Morocco.*
**Corresponding author:* Abdelhay Laabyech; Email: abdelhay.laabyech@gmail.com.

formation, but leads to poor nutrient distribution, which reduces agitation in the digester, compromises anaerobic digestion performance and reduces the rate of biogas production [18]. However, mixed digesters produce more biogas than unmixed digesters. Various techniques are used to ensure mixing in the anaerobic digester, such as the use of mechanical agitators (scrapers, pistons, etc.) or recirculation systems for the substrate or the gas produced using pumps [8, 19]. In the case of continuous digesters, agitation can also be provided by the incoming flow [7, 17]. Furthermore, understanding and optimising the phenomenon of anaerobic digestion requires in-depth analysis. There are therefore several techniques for optimising the anaerobic digestion process, such as traditional control methods and methods based on mathematical modelling and numerical simulation. The first are easy to implement and are based on experience and rules of thumb. They require the use of real-time sensors to monitor and adjust reaction conditions in order to optimise production. The second type requires modelling, simulation and data processing skills. They take into account multiple variables and complex interactions, enabling biogas production to be maximised more efficiently [20, 21].

Modelling the anaerobic digestion process is a very powerful tool that allows us to understand complex phenomena, determine certain kinetic parameters that are difficult to access through experimentation, predict degradation kinetics and the dynamic evolution of environments, optimise operating parameters and biogas production, reduce operating costs and minimise environmental impact [21]. Like other approaches, the modelling of anaerobic digestion has its own constraints and limitations. These include the fact that modelling the biological process is highly complex and requires highly coupled non-linear mathematical equations, the numerical resolution of which therefore requires powerful computing machines. Because of the importance of anaerobic digestion, several dynamic models have been developed. The complexity of these models varies according to the number of biochemical and physicochemical processes involved [22]. They generally propose a commonly accepted hypothesis that links kinetic models of degradation to biological models of growth. The latter consider that the substrate is transformed into products by the presence of a bacterial population. Thus, these anaerobic digestion models are based on principles such as the conservation of matter [22]. In fact, The differences between these anaerobic digestion models are mainly linked to the choice of representation of bacterial kinetics [22]. The main variables to be determined in our study are velocity, temperature and concentration. These variables are obtained by solving the system of equations presented in section 4.

In this work, we focus on the amount of biogas produced by the anaerobic digestion of soluble organic matter in the effluent of a pulp and paper mill. Its main objective is to examine and analyse the evolution of the physical and biological parameters that characterize it. To understand fluid dynamics within the anaerobic digester and improve biogas production. In addition, several authors [23, 24] have considered the fluid to be incompressible, neglecting the amount of gas produced during the anaerobic digestion process. With this in mind, a characterisation of the digester was carried out in both cases, compressible and incompressible, in order to determine whether the gas produced during the process had any impact on the characteristics of the fluid inside the digester. In addition, a comparison was made between the results obtained for the compressible and incompressible cases in order to simplify similar study cases. In this context, biogas production was modelled using the mathematical model created by (El Fadel and al. [25]; Vavilin and al. [26]; Men-La-Yakhaf and al. [27]). In addition, the modelling of fluid dynamics within the digester was based on the conservative equations (mass, momentum and energy) [28].

2. METHODOLOGY

The various treatments used at the WWTP, the physico-chemical and biological parameters, the experimental conditions of the treated effluent and the quantities of biogas measured at the digester outlet are presented in section 3. The mathematical formulation of the conservative equations and the kinetic model of biogas production is given in section 4. Section 5 will focus on simulating the aforementioned equations. The corresponding results are presented in Figures 3 to 11, while their analysis and discussion will take place in Section 6.

3. TREATMENTS USED AND PARAMETERS OBTAINED AT DIFFERENT LEVELS OF THE WWTP

The treatment plant can treat an average of 4500 m^3 of liquid effluent from the pulp and paper mills per day [29]. These effluents, before being discharged into the environment, are subjected to a primary treatment followed by a secondary treatment [7, 30].

3.1. Treatments used

3.1.1. Primary treatment

The primary treatment allows the separation of large particles from the effluent discharged by the plant [7, 29]. This operation takes place first in a clarifier, which is a round tank fitted with a rotating scraper bridge that operates continuously. This bridge allows to push the decanted pulp towards a central well located in the basin. Then, due to hydrostatic pressure, the pulp is discharged from the basin. The effluent then passes through a

dissolved air flotation tank, which separates suspended solids and colloidal solids from the effluent by flotation, reducing their apparent density [29]. This technique is achieved by dissolving the air in the wastewater under pressure, then releasing the air at atmospheric pressure into the flotation tank. When air bubbles are combined with solid or liquid particles, they form densities lower than those of water and float [29, 30].

3.1.2. Secondary treatment

The clarified water is adjusted to the optimal conditions for the anaerobic digestion process. First, the water is passed through a heat exchanger so that its temperature becomes suitable for the downstream treatment. as well as through a conditioning tower that ensures nutritional balance and pH adjustment to create an optimal environment for the growth and development of microorganisms [31, 32]. This water then undergoes a secondary treatment, an anaerobic biological treatment in the digester, which breaks down and transforms the biodegradable organic matter (Carbohydrates, Lipids, and Proteins) by micro-organisms into a gas, rich in methane. The gas produced in the digester is evacuated via evacuation channels located at the top of the digester [6, 29, 33]. After passing through the digester, the water undergoes purification, ensuring its release into the river with a composition that maintains the equilibrium of the aquatic ecosystem intact.

3.2. Physical, chemical and biological parameters of the WWTP

The results of the physical, chemical and biological parameters obtained during the primary and secondary treatment of liquid effluent are measured at several points in the treatment plant.

In the clarifier and air flotation unit, the effluent maintains an acidic pH, whereas it is neutral in the anaerobic digester, with a value of 7.2 This change is due to the adjustments made to the effluent in the conditioning tower. Thus, the temperature measured in the digester is 30°C. These two quantities are appropriate and favourable for the mesophilic microorganisms to thrive in the digester [29].

When the effluent passes from the clarifier to the flotation tank, there is a slight decrease in COD of around 1%, from a value of 2118 mg/L to 2092 mg/L. whereas, it decreases considerably, to a value of 600 mg/L, after passing through the digester. This decrease is due to the oxidation of the organic substances within the effluent

In addition, the biological treatment in the anaerobic digester ensures a considerable reduction of the BOD to a value of 200 mg/l. this decrease is due to the degradation and transformation of the organic substances within the effluent by anaerobic micro-organisms [29].

3.3. Daily biogas production

The daily biogas production measured at the outlet of the anaerobic digester is shown in Figure 1. This production experiences daily variations depending on the organic matter concentration in the effluent and the hydraulic retention time [34]. A longer retention time will allow greater biodegradation and increase biogas production. This explains the production achieved on the fourth day after the two-day shutdown reserved for maintenance of the machinery and the entire plant [29].

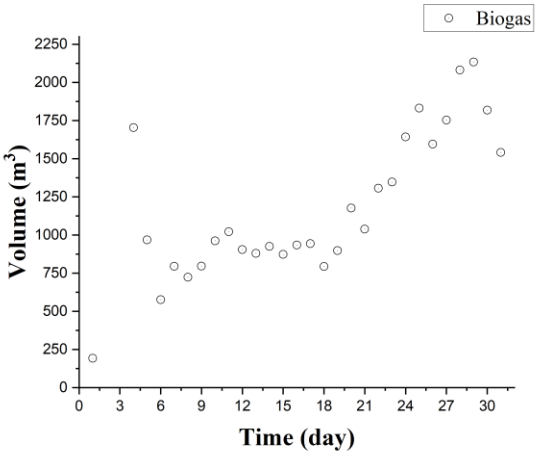

Fig. 1. Biogas produced during one month [29].

4. MATHEMATICAL FORMULATION

The primary aim is to model the flow in the digester, taking into account the biogas production. To this end, we present below the equations of conservation of matter, momentum, and energy, as well as a set of mathematical equations governing biodegradation and biogas generation, under the following assumptions:

- The flow is in a digester with a cylindrical shape. In this situation, it is more convenient to express the equation in a cylindrical coordinate system with a velocity field $\vec{u} = (r, \theta, z, t)$;

- The flow is a homogeneous and axisymmetric fluid flow:

$$\frac{\partial}{\partial \theta} = 0 \text{ and } u_\theta = 0 ;$$

- The components of the velocity vector are:

$$\vec{u} = \begin{cases} u_r = u_r(r,z,t) \\ u_\theta = 0 \\ u_z = u_z(r,z,t) \end{cases} \rightarrow \quad \vec{u} = u_r(r,z,t)\vec{e}_r + u_z(r,z,t)\vec{e}_z$$

4.1. Fluid dynamics in the digester

- Conservation of mass

The mass conservation equation, for a volume in which mass enters and goes out with a generation of internal density per unit of time in the compressible and incompressible cases; is written as follows:

$$\text{Compressible: } \frac{\partial \rho_{fluid}}{\partial t} + div(\rho_{fluid} u) = \Gamma \quad (1)$$

$$\text{Incompressible: } \rho_{fluid} div(u) = \Gamma \quad (2)$$

- Conservation of momentum

For a Newtonian fluid and the resulting equations of momentum are those of Navier-Stokes. In the compressible and incompressible cases these equations are written as follows:

Compressible:

$$\rho \frac{d\vec{u}}{dt} = \rho\left[\frac{\partial \vec{u}}{\partial t} + (\vec{u}.\nabla)\vec{u}\right] = \vec{f} - \nabla p - \frac{2}{3}(\mu \nabla.\vec{u}) + \nabla.\left[\mu\left(\nabla\vec{u} + (\nabla\vec{u})^T\right)\right] \quad (3)$$

Incompressible:

$$\rho \frac{d\vec{u}}{dt} = \rho\left[\frac{\partial \vec{u}}{\partial t} + (\vec{u}.\nabla)\vec{u}\right] = \vec{f} - \nabla p - \mu \nabla^2 \vec{u} \quad (4)$$

- Conservation of energy

$$\rho C_p \frac{DT}{Dt} = \rho C_p \frac{\partial T}{\partial t} + \rho C_p \nabla.(\vec{u}T) = \rho \dot{q}_g + K\nabla^2 T + \phi + S \quad (5)$$

where the viscous dissipation rate:

Compressible:

$$\phi = 2\mu\left[\left(\frac{\partial u_r}{\partial r}\right)^2 + \left(\frac{1}{r}\frac{\partial u_\theta}{\partial \theta} + \frac{u_r}{r}\right)^2 + \left(\frac{\partial u_z}{\partial z}\right)^2\right] - \frac{2}{3}\mu\left(\frac{1}{r}\frac{\partial (r u_r)}{\partial r} + \frac{1}{r}\frac{\partial u_\theta}{\partial \theta} + \frac{\partial u_z}{\partial z}\right)^2 + \mu\left[\begin{array}{l}\left(\frac{1}{r}\frac{\partial u_r}{\partial \theta} + \frac{\partial u_\theta}{\partial r} - \frac{u_\theta}{r}\right)^2 + \\ \left(\frac{\partial u_\theta}{\partial z} + \frac{1}{r}\frac{\partial u_z}{\partial \theta}\right)^2 + \\ \left(\frac{\partial u_z}{\partial r} + \frac{\partial u_r}{\partial z}\right)^2\end{array}\right] \quad (6)$$

Incompressible:

$$\phi = 2\mu\left[\left(\frac{\partial u_r}{\partial r}\right)^2 + \left(\frac{1}{r}\frac{\partial u_\theta}{\partial \theta} + \frac{u_r}{r}\right)^2 + \left(\frac{\partial u_z}{\partial z}\right)^2\right] + \mu\left[\begin{array}{l}\left(\frac{1}{r}\frac{\partial u_r}{\partial \theta} + \frac{\partial u_\theta}{\partial r} - \frac{u_\theta}{r}\right)^2 + \\ \left(\frac{\partial u_\theta}{\partial z} + \frac{1}{r}\frac{\partial u_z}{\partial \theta}\right)^2 + \\ \left(\frac{\partial u_z}{\partial r} + \frac{\partial u_r}{\partial z}\right)^2\end{array}\right] \quad (7)$$

By projection and using the above assumptions, the equations (1-5) become:

- Conservation of mass

For compressible fluids

$$\frac{\partial \rho}{\partial t} + \frac{1}{r}\frac{\partial(\rho\, r u_r)}{\partial r} + \frac{\partial(\rho\, u_z)}{\partial z} = \Gamma \quad (8)$$

For incompressible fluids

$$\frac{1}{r}\rho\frac{\partial(r u_r)}{\partial r} + \rho\frac{\partial(u_z)}{\partial z} = \Gamma \quad (9)$$

- Conservation of Momentum

In the radial direction:

For compressible fluids

$$\rho\left(\frac{\partial u_r}{\partial t} + u_r\frac{\partial u_r}{\partial r} + u_z\frac{\partial u_r}{\partial z}\right) = \frac{\partial}{\partial r}\left[\mu\left(-\frac{2}{3}\left(\frac{u_r}{r} + \frac{\partial u_r}{\partial r} + \frac{\partial u_z}{\partial z}\right) + 2\frac{\partial u_r}{\partial r}\right)\right] + \frac{\partial}{\partial z}\left[\mu\left(\frac{\partial u_r}{\partial z} + \frac{\partial u_z}{\partial r}\right)\right] + \frac{2\mu}{r}\left(\frac{\partial u_r}{\partial r} - \frac{u_r}{r}\right) \quad (10)$$

In the axial direction:

For compressible fluids

$$\rho\left(\frac{\partial u_z}{\partial t} + u_r\frac{\partial u_z}{\partial r} + u_z\frac{\partial u_z}{\partial z}\right) = -\frac{\partial p}{\partial z} + \rho g_z + \frac{\mu}{r}\left(\frac{\partial u_z}{\partial r} + \frac{\partial u_r}{\partial z}\right) + \frac{\partial}{\partial r}\left[\mu\left(\frac{\partial u_r}{\partial z} + \frac{\partial u_z}{\partial r}\right)\right] + \frac{\partial}{\partial z}\left[\mu\left(-\frac{2}{3}\left(\frac{u_r}{r} + \frac{\partial u_r}{\partial r} + \frac{\partial u_z}{\partial z}\right) + 2\frac{\partial u_z}{\partial z}\right)\right] \quad (11)$$

For incompressible fluids

$$\rho\left(\frac{\partial u_z}{\partial t} + u_r\frac{\partial u_z}{\partial r} + u_z\frac{\partial u_z}{\partial z}\right) = -\frac{\partial p}{\partial z} - \rho g_z + \mu\left[\left(\frac{1}{r}\frac{\partial}{\partial r}\left(r\frac{\partial u_z}{\partial r}\right) + \frac{\partial^2 u_z}{\partial z^2}\right)\right] \quad (12)$$

- Conservation of energy

For compressible fluids:

$$\rho C_p\left[\frac{\partial T}{\partial t}+u_r\frac{\partial T}{\partial r}+\frac{\partial T}{\partial z}\right]= \rho\dot{q}_g+\frac{1}{r}\frac{\partial}{\partial r}\left(kr\frac{\partial T}{\partial r}\right)+\frac{\partial}{\partial z}\left(k\frac{\partial T}{\partial z}\right)+\phi+S \quad (13)$$

where:

$$\phi=2\mu\left[\left(\frac{\partial u_r}{\partial r}\right)^2+\left(\frac{u_r}{r}\right)^2+\left(\frac{\partial u_z}{\partial z}\right)^2\right]+ \mu\left[\left(\frac{\partial u_z}{\partial r}+\frac{\partial u_r}{\partial z}\right)^2\right]-\frac{2}{3}\mu\left(\frac{1}{r}\frac{\partial(ru_r)}{\partial r}+\frac{\partial u_z}{\partial z}\right)^2$$

For incompressible fluids

$$\rho C_p\left[\frac{\partial T}{\partial t}+u_r\frac{\partial T}{\partial r}+\frac{\partial T}{\partial z}\right]= \rho\dot{q}_g+\frac{1}{r}\frac{\partial}{\partial r}\left(kr\frac{\partial T}{\partial r}\right)+\frac{\partial}{\partial z}\left(k\frac{\partial T}{\partial z}\right)+\phi+S \quad (14)$$

where:

$$\phi=2\mu\left[\left(\frac{\partial u_r}{\partial r}\right)^2+\left(\frac{u_r}{r}\right)^2+\left(\frac{\partial u_z}{\partial z}\right)^2\right]+\mu\left(\frac{\partial u_z}{\partial r}+\frac{\partial u_r}{\partial z}\right)^2$$

4.2. Biogas production model

To model biogas production, we opted to use a mathematical model that describes the dynamics of the waste degradation ecosystem. This model relies on the Monod model to describe microbial growth. It includes the hydrolysis phase, taking into account the kinetics of hydrolysis. As well as the acidogenesis, acetogenesis and methanogenesis phases (figure 2) [25, 35, 36].

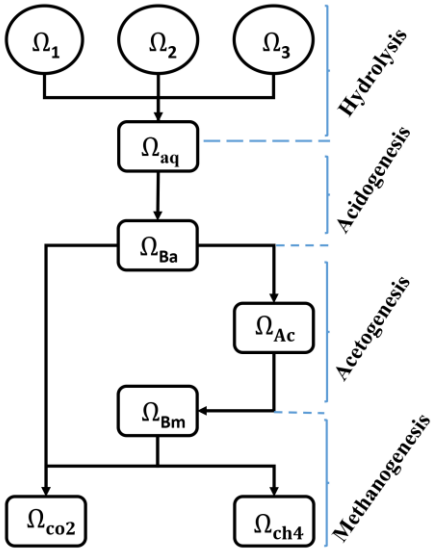

Fig. 2. Diagram of the biogas production model [35].

The equations of the mathematical model represent the transformation of complex molecules into simpler ones. The birth and death of acidogenic and methanogenic biomass. The production of acetate which is metabolized into methane. Finally, the production of methane and carbon dioxide by all the steps of anaerobic digestion. These equations are expressed as a system of coupled first order differential equations of the form:

Organic carbon: $$\frac{d\Omega_i}{dt}=-\sum_{i=1}^{3}(h_i\Omega_i) \quad (15)$$

Aqueous organic carbon:

$$\frac{d\Omega_{aq}}{dt}=\sum_{i=1}^{3}(h_i\Omega_i)-\left[\left(\frac{\lambda_a}{Y_A}\right)\left(\frac{\Omega_{aq}}{H_{Sa}+\Omega_{aq}}\right)\Omega_{Ba}\right] \quad (16)$$

Acidogenic biomass carbon:

$$\frac{d\Omega_{Ba}}{dt}=\left[\left(\frac{\lambda_a.\Omega_{aq}}{H_{Sa}+\Omega_{aq}}\right)-D_a\right].\Omega_{Ba} \quad (17)$$

Methanogenic biomass carbon:

$$\frac{d\Omega_{Bm}}{dt}=\left[\left(\frac{\lambda_M.\Omega_{ac}}{H_{Sa}+\Omega_{Ac}}\right)-D_m\right].\Omega_{Bm} \quad (18)$$

Acetate carbon:

$$\frac{d\Omega_{Ac}}{dt}=-\left[\left(\frac{\lambda_m}{Y_M}\right)\left(\frac{\Omega_{Ac}}{H_{Sm}+\Omega_{Ac}}\right)\right]\Omega_{Bm}+ Y_{Ac}\left[(1-Y_A)\left(\frac{\lambda_A}{Y_A}\right)\left(\frac{\Omega_{aq}}{H_{Sa}+\Omega_{aq}}\right)+D_a\right]\Omega_{Ba} \quad (19)$$

Methane carbon:

$$\frac{d\Omega_{CH_4}}{dt}= Y_{CH_4}\left[(1-Y_M)\left(\frac{\lambda_M}{Y_M}\right)\left(\frac{\Omega_{Ac}}{H_{Sm}+\Omega_{Ac}}\right)+D_a\right]\Omega_{Bm} \quad (20)$$

Carbon dioxide carbon:

$$\frac{d\Omega_{CO_2}}{dt}=(1-Y_{CH_4})\left[(1-Y_M)\left(\frac{\lambda_M}{Y_M}\right)\left(\frac{\Omega_{Ac}}{H_{Sm}+\Omega_{Ac}}\right)\right]\Omega_{Bm}+ (1-Y_{Ac})\left[(1-Y_A)\left(\frac{\lambda_A}{Y_A}\right)\left(\frac{\Omega_{aq}}{H_{Sa}+\Omega_{aq}}\right)+D_a\right]\Omega_{Ba} \quad (21)$$

5. NUMERICAL RESOLUTION

In this modelling, the conservative mass, momentum and energy equations (equations 8-14) have been solved by the finite volume method coupled with the Gauss-Seidel method [37]–[39].

The finite volume method is a well suited and often used method for solving conservation laws because it

requires that the flow into a control volume is equal to the flow out of the adjacent volume. Furthermore, the finite volume method, employing the Navier-Stokes equations, provides accurate and stable numerical solutions for complex fluid dynamics problems. Thus, by using unstructured meshes, this method allows to solve partial differential equations with complex geometry.

The Gauss-Seidel method is an iterative method that we will use to solve the system of algebraic equations obtained by the finite volume method.

This method consumes less machine memory resources and often converges faster than other iterative methods for solving linear systems.

The mathematical equations 15-21 have no analytical solution, and their resolution requires the application of numerical methods. Indeed, the equations of the system, which depend only on time, are ordinary differential equations, justifying the use of an iterative method such as the second-order Runge-Kutta method. Moreover, this method enabled the transformation of the system of equations into a set of algebraic equations. [27, 35].

5.1. Conservative equations

In what follows, we will integrate the system equations 8-14 over the control volume (r dr dz) and the time interval dt, employing the implicit finite volume method.

- Conservation of mass

For compressible fluids:

$$\int_{vc}\int_{dt}\frac{\partial \rho}{\partial t}\ \mathrm{r}drdzdt+\int_{vc}\int_{dt}\rho\frac{u_r}{r}\ \mathrm{r}drdzdt+\int_{vc}\int_{dt}\frac{\partial(\rho u_r)}{\partial r}\ \mathrm{r}drdzdt+\int_{vc}\int_{dt}\frac{\partial(\rho u_z)}{\partial z}\ \mathrm{r}drdzdt=\int_{vc}\int_{dt}\Gamma\ \mathrm{r}drdzdt \quad (22)$$

The equation becomes

$$r_p\left[(\rho)_P^{t+dt}-(\rho)_P^{t}\right]\Delta r\Delta z+\rho_P^{t+dt}\ (u_r)_P\ \Delta r\Delta z\Delta t+(u_r)_P\ r_P\left[(\rho)_E^{t+dt}-(\rho)_O^{t+dt}\right]\frac{\Delta z\ \Delta t}{2}+(u_z)_P\ r_P\left[(\rho)_N^{t+dt}+(\rho)_S^{t+dt}\right]\frac{\Delta r\ \Delta t}{2}=\bar{\Gamma}^{t+dt}\ \mathrm{r}_p\Delta r\Delta z\Delta t \quad (23)$$

The equation can therefore be formulated as follows:

$$A(i,j)(\rho)_{(i+1,j)}^{k+1}+B(i,j)(\rho)_{(i-1,j)}^{k+1}+C(i,j)(\rho)_{(i,j)}^{k+1}+E(i,j)(\rho)_{(i,j+1)}^{k+1}+F(i,j)(\rho)_{(i,j-1)}^{k+1}=D(i,j)$$

where:

$$A(i,j)=r_P(u_r)_P\frac{\Delta z\ \Delta t}{2}$$

$$B(i,j)=-r_P(u_r)_P\frac{\Delta z\ \Delta t}{2}$$

$$C(i,j)=r_p\ \Delta r\Delta z+(u_r)_p\ \Delta r\Delta z\Delta t$$

$$D(i,j)=\bar{\Gamma}^{t+dt}\ \mathrm{r}_p\ \Delta r\ \Delta z\ \Delta t+(\rho)_P^{t}\ r_p\Delta r\Delta z$$

$$E(i,j)=r_p(u_z)_P\frac{\Delta r\ \Delta t}{2}$$

$$F(i,j)=-r_p(u_z)_P\frac{\Delta r\ \Delta t}{2}$$

For incompressible fluids:

$$\int_{vc}\int_{dt}\rho\frac{\partial u_r}{\partial r}\ \mathrm{r}drdzdt+\int_{vc}\int_{dt}\rho\frac{u_r}{r}\ \mathrm{r}drdzdt+\int_{vc}\int_{dt}\rho\frac{\partial u_z}{\partial z}\ \mathrm{r}drdzdt=\int_{vc}\int_{dt}\Gamma\ \mathrm{r}drdzdt \quad (24)$$

The equation becomes

$$r_p\rho_P\left[(u_z)_N^{t+dt}-(u_z)_S^{t+dt}\right]\frac{\Delta r\Delta t}{2}+\rho_P(u_r)_P^{t+dt}\ \Delta r\Delta z\Delta t+r_p\rho_P\left[(u_r)_E^{t+dt}-(u_r)_O^{t+dt}\right]\frac{\Delta z\Delta t}{2}=\bar{\Gamma}^{t+dt}\ \mathrm{r}_p\ \Delta r\Delta z\Delta t \quad (25)$$

The equation can therefore be formulated as follows

$$A(i,j)(u_r)_{(i+1,j)}^{k+1}+B(i,j)(u_r)_{(i-1,j)}^{k+1}+C(i,j)(u_r)_{(i,j)}^{k+1}+E(i,j)(u_r)_{(i,j+1)}^{k+1}+F(i,j)(u_r)_{(i,j-1)}^{k+1}=D(i,j)$$

where:

$$A(i,j)=r_P\rho_P\frac{\Delta z\ \Delta t}{2}$$

$$B(i,j)=-r_P\rho_P\frac{\Delta z\ \Delta t}{2}$$

$$C(i,j)=\rho_P\Delta r\Delta z\Delta t$$

$$D(i,j)=\bar{\Gamma}^{t+dt}\ \mathrm{r}_p\ \Delta r\ \Delta z\ \Delta t$$

$$E(i,j)=r_P\rho_P\frac{\Delta r\ \Delta t}{2}$$

$$F(i,j)=-r_P\rho_P\frac{\Delta r\ \Delta t}{2}$$

- Conservation of momentum

In the radial direction:

For compressible fluids

$$\int_{vc}\int_{dt}\rho\frac{\partial u_r}{\partial t}\mathrm{r}drdzdt+\int_{vc}\int_{dt}\rho u_r\frac{\partial u_r}{\partial r}\ \mathrm{r}\ dr\ dz\ dt+$$
$$\int_{vc}\int_{dt}\rho u_z\frac{\partial u_r}{\partial z}\mathrm{r}drdzdt=\int_{vc}\int_{dt}\frac{\partial}{\partial r}\left(2\mu\frac{\partial u_r}{\partial r}\right)\mathrm{r}drdzdt+$$
$$\int_{vc}\int_{dt}-\frac{2\mu}{3}\frac{\partial}{\partial r}\left(\frac{\partial u_r}{\partial r}\right)\mathrm{r}drdzdt+\int_{vc}\int_{dt}-\frac{2\mu}{3}\frac{1}{r}\frac{\partial u_r}{\partial r}\mathrm{r}drdzdt+$$
$$\int_{vc}\int_{dt}\frac{2\mu}{3}\frac{u_r}{r^2}\mathrm{r}drdzdt+\int_{vc}\int_{dt}\frac{\partial}{\partial r}\left(-\frac{2\mu}{3}\frac{\partial u_z}{\partial z}\right)\mathrm{r}drdzdt+ \quad (26)$$
$$\int_{vc}\int_{dt}\frac{\partial}{\partial z}\left(\mu\frac{\partial u_r}{\partial z}\right)\mathrm{r}drdzdt+\int_{vc}\int_{dt}\frac{\partial}{\partial z}\left(\mu\frac{\partial u_z}{\partial r}\right)\mathrm{r}drdzdt+$$
$$\int_{vc}\int_{dt}\frac{2\mu}{r}\frac{\partial u_r}{\partial r}r\ dr\ dz\ dt+\int_{vc}\int_{dt}-2\mu\frac{u_r}{r^2}r\ dr\ dz\ dt$$

The equation becomes:

$$\rho_P r_P\left[\left(u_r\right)_P^{t+dt}-\left(u_r\right)_P^{t}\right]\Delta r\Delta z+$$
$$r_P\rho_P\left(u_r\right)_p\left[\left(u_r\right)_E^{t+dt}-\left(u_r\right)_O^{t+dt}\right]\frac{\Delta z\Delta t}{2}+$$
$$r_P\rho_P\left(u_z\right)_p\left[\left(u_r\right)_N^{t+dt}-\left(u_r\right)_S^{t+dt}\right]\frac{\Delta r\Delta t}{2}=$$
$$-\frac{\mu}{3}\left[\left(u_r\right)_E^{t+dt}-\left(u_r\right)_O^{t+dt}\right]\Delta z\Delta t+$$
$$2\mu r_p\left[\left(u_r\right)_E^{t+dt}-2\left(u_r\right)_P^{t+dt}+\left(u_r\right)_O^{t+dt}\right]\frac{\Delta z\Delta t}{\Delta r}- \quad (27)$$
$$\frac{2\mu}{3}r_p\left[\left(u_r\right)_E^{t+dt}-2\left(u_r\right)_P^{t+dt}+\left(u_r\right)_O^{t+dt}\right]\frac{\Delta z\Delta t}{\Delta r}+$$
$$\frac{2\mu}{3}\frac{1}{r_P}\left(u_r\right)_P^{t+dt}\Delta r\ \Delta z\ \Delta t-\frac{2\mu}{r_P}\left(u_r\right)_P^{t+dt}\Delta r\Delta z\Delta t+$$
$$\mu r_p\left[\left(u_r\right)_N^{t+dt}-2\left(u_r\right)_P^{t+dt}+\left(u_r\right)_S^{t+dt}\right]\frac{\Delta r\Delta t}{\Delta z}+$$
$$\mu r_P\left[\frac{\partial}{\partial z}\left(\frac{\partial u_z}{\partial r}\right)\right]_P\Delta r\Delta z\Delta t-$$
$$\frac{2\mu}{3}\mathrm{r}_P\left[\frac{\partial}{\partial r}\left(\frac{\partial u_z}{\partial z}\right)\right]_P\Delta r\Delta z\Delta t\ +$$
$$\mu\left[\left(u_r\right)_E^{t+dt}-\left(u_r\right)_O^{t+dt}\right]\Delta z\Delta t$$

The equation can therefore be formulated as follows:

$$A(i,j)\left(u_r\right)_{(i+1,j)}^{k+1}+B(i,j)\left(u_r\right)_{(i-1,j)}^{k+1}+C(i,j)\left(u_r\right)_{(i,j)}^{k+1}+$$
$$E(i,j)\left(u_r\right)_{(i,j+1)}^{k+1}+F(i,j)\left(u_r\right)_{(i,j-1)}^{k+1}=D(i,j)$$

where:

$$A(i,j)=-\frac{4}{3}\mu r_P\frac{\Delta z\ \Delta t}{\Delta r}-\frac{2}{3}\mu\Delta z\ \Delta t+r_P\rho_P\left(u_r\right)_P\frac{\Delta z\ \Delta t}{2}$$

$$B(i,j)=-\frac{4}{3}\mu r_P\frac{\Delta z\ \Delta t}{\Delta r}+\frac{2}{3}\mu\Delta z\ \Delta t-r_P\rho_P\left(u_r\right)_P\frac{\Delta z\ \Delta t}{2}$$

$$C(i,j)=r_P\rho_P\ \Delta r\ \Delta z+\frac{8}{3}\mu r_P\frac{\Delta z\ \Delta t}{\Delta r}+2\mu\ r_p\frac{\Delta r\ \Delta t}{\Delta z}+$$
$$\frac{4}{3}\frac{\mu}{r_P}\Delta r\ \Delta z\ \Delta t$$

$$D(i,j)=\rho_P r_p\left(u_r\right)_P^{t}\Delta r\Delta z+\frac{1}{3}\mu r_P\left(\frac{\partial}{\partial z}\left(\frac{\partial u_z}{\partial r}\right)\right)_P\Delta r\Delta z\Delta t$$

$$E(i,j)=-\mu r_P\frac{\Delta r\ \Delta t}{\Delta z}+\rho_P r_P\left(u_z\right)_P\frac{\Delta r\ \Delta t}{2}$$

$$F(i,j)=-\mu r_P\frac{\Delta r\ \Delta t}{\Delta z}-\rho_P r_P\left(u_z\right)_P\frac{\Delta r\ \Delta t}{2}$$

In the axial direction:

For compressible fluids

$$\int_{vc}\int_{dt}\rho\frac{\partial u_z}{\partial t}\ \mathrm{r}\ dr\ dz\ dt+\int_{vc}\int_{dt}\rho u_r\frac{\partial u_z}{\partial r}\ \mathrm{r}\ dr\ dz\ dt+$$
$$\int_{vc}\int_{dt}\rho u_z\frac{\partial u_z}{\partial z}\ \mathrm{r}\ dr\ dz\ dt=\int_{vc}\int_{dt}-\frac{\partial p}{\partial z}\ \mathrm{r}\ dr\ dz\ dt+$$
$$\int_{vc}\int_{dt}-\rho g_z\ \mathrm{r}\ dr\ dz\ dt+\frac{2\mu}{3}\int_{vc}\int_{dt}\frac{u_r}{r^2}\mathrm{r}\ dr\ dz\ dt-$$
$$\int_{vc}\int_{dt}\frac{2\mu}{3}\frac{\partial}{\partial z}\left(\frac{\partial u_r}{\partial r}\right)\mathrm{r}drdzdt-\int_{vc}\int_{dt}\frac{2\mu}{3}\frac{1}{r}\frac{\partial u_r}{\partial z}\mathrm{r}drdzdt- \quad (28)$$
$$\int_{vc}\int_{dt}\frac{2\mu}{3}\frac{\partial}{\partial z}\left(\frac{\partial u_z}{\partial z}\right)\mathrm{r}drdzdt+\int_{vc}\int_{dt}\frac{\mu}{r}\frac{\partial u_r}{\partial z}\mathrm{r}drdzdt+$$
$$\int_{vc}\int_{dt}\mu\frac{\partial}{\partial r}\left(\frac{\partial u_r}{\partial z}\right)\mathrm{r}drdzdt+\int_{vc}\int_{dt}\mu\frac{\partial}{\partial r}\left(\frac{\partial u_z}{\partial r}\right)\mathrm{r}drdzdt+$$
$$\int_{vc}\int_{dt}\frac{\mu}{r}\frac{\partial u_z}{\partial r}\ \mathrm{r}\ dr\ dz\ dt+\int_{vc}\int_{dt}2\mu\frac{\partial}{\partial z}\left(\frac{\partial u_z}{\partial z}\right)\mathrm{r}drdzdt$$

The equation becomes:

$$\rho_P r_P\left[\left(u_z\right)_P^{t+dt}-\left(u_z\right)_P^{t}\right]\Delta r\Delta z+$$
$$\rho_P r_P\left(u_r\right)_p\left[\left(u_z\right)_E^{t+dt}-\left(u_z\right)_O^{t+dt}\right]\frac{\Delta z\Delta t}{2}+ \quad (29)$$
$$\rho_P r_P\left(u_z\right)_p\left[\left(u_z\right)_N^{t+dt}-\left(u_z\right)_S^{t+dt}\right]\frac{\Delta r\Delta t}{2}=$$

$$-r_p\left(\frac{\partial p}{\partial z}\right)_P \Delta r\Delta z\Delta t - \frac{2\mu}{3}\left(\frac{\partial u_r}{\partial z}\right)_P \Delta r\Delta z\Delta t -$$
$$g_z\rho_P r_P \Delta r\Delta z\Delta t + \frac{2\mu}{3}\frac{1}{r_P}(u_r)_P \Delta r\Delta z\Delta t -$$
$$\frac{2\mu}{3} r_P\left[\frac{\partial}{\partial z}\left(\frac{\partial u_r}{\partial r}\right)\right]_P \Delta r\Delta z\Delta t + \mu\left(\frac{\partial u_r}{\partial z}\right)_P \Delta r\Delta z\Delta t -$$
$$\frac{2\mu}{3} r_P\left[(u_z)_N^{t+dt} - 2(u_z)_P^{t+dt} + (u_z)_S^{t+dt}\right]\frac{\Delta r\Delta t}{\Delta z} +$$
$$2\mu r_p\left[(u_z)_N^{t+dt} - 2(u_z)_P^{t+dt} + (u_z)_S^{t+dt}\right]\frac{\Delta r\Delta t}{\Delta z} +$$
$$\mu\left[(u_z)_E^{t+dt} - (u_z)_O^{t+dt}\right]\frac{\Delta z\Delta t}{2} + \mu r_P\left[\frac{\partial}{\partial r}\left(\frac{\partial u_r}{\partial z}\right)\right]_p \Delta r\Delta z\Delta t +$$
$$\mu r_P\left[(u_z)_E^{t+dt} - 2(u_z)_P^{t+dt} + (u_z)_O^{t+dt}\right]\frac{\Delta z\Delta t}{\Delta r}$$

The equation can therefore be formulated as follows:

$$A(i,j)(u_z)_{(i+1,j)}^{k+1} + B(i,j)(u_z)_{(i-1,j)}^{k+1} + C(i,j)(u_z)_{(i,j)}^{k+1} +$$
$$E(i,j)(u_z)_{(i,j+1)}^{k+1} + F(i,j)(u_z)_{(i,j-1)}^{k+1} = D(i,j)$$

where:

$$A(i,j) = -\mu r_P\frac{\Delta z\ \Delta t}{\Delta r} - \mu\frac{\Delta z\ \Delta t}{2} + r_P\rho_P(u_r)_p\frac{\Delta z\ \Delta t}{2}$$

$$B(i,j) = -\mu r_P\frac{\Delta z\ \Delta t}{\Delta r} + \mu\frac{\Delta z\ \Delta t}{2} - r_P\rho_P(u_r)_p\frac{\Delta z\ \Delta t}{2}$$

$$C(i,j) = \rho_P r_p\Delta r\ \Delta z + \frac{8}{3}\mu r_P\frac{\Delta r\ \Delta t}{\Delta z} + 2\mu r_p\frac{\Delta z\ \Delta t}{\Delta r}$$

$$D(i,j) = \rho_P r_p(u_z)_p^t\ \Delta r\Delta z + \frac{2\mu}{3}\frac{(u_r)_P}{r_P}\Delta r\ \Delta z\ \Delta t +$$
$$\frac{1}{3}\mu\left(\frac{\partial u_r}{\partial z}\right)_P \Delta r\Delta z\Delta t + \frac{1}{3}\mu r_P\left[\frac{\partial}{\partial z}\left(\frac{\partial u_r}{\partial r}\right)\right]_P \Delta r\Delta z\Delta t -$$
$$r_p\left(\frac{\partial p}{\partial z}\right)_P \Delta r\ \Delta z\ \Delta t - g_r r_P\rho_P\ \Delta r\ \Delta z\ \Delta t$$

$$E(i,j) = -\frac{4\mu}{3} r_P\frac{\Delta r\ \Delta t}{\Delta z} + r_P\rho_P(u_z)_P\frac{\Delta r\ \Delta t}{2}$$

$$F(i,j) = -\frac{4\mu}{3} r_P\frac{\Delta r\ \Delta t}{\Delta z} - r_P\rho_P(u_z)_P\frac{\Delta r\ \Delta t}{2}$$

For incompressible fluids

$$\int_{vc}\int_{dt}\rho\frac{\partial u_z}{\partial t}\,\mathrm{r}drdzdt + \int_{vc}\int_{dt}\rho u_r\frac{\partial u_z}{\partial r}\,\mathrm{r}drdzdt +$$
$$\int_{vc}\int_{dt}\rho u_z\frac{\partial u_z}{\partial z}\,\mathrm{r}drdzdt = \int_{vc}\int_{dt} -\frac{\partial p}{\partial z}\,\mathrm{r}drdzdt -$$
$$\int_{vc}\int_{dt}\rho g_z\ \mathrm{r}drdzdt + \int_{vc}\int_{dt}\mu\frac{\partial^2 u_z}{\partial r^2}\,\mathrm{r}drdzdt + \quad (30)$$
$$\int_{vc}\int_{dt}\mu\frac{1}{r}\frac{\partial u_z}{\partial r}\,\mathrm{r}drdzdt + \int_{vc}\int_{dt}\mu\frac{\partial^2 u_z}{\partial z^2}\,\mathrm{r}drdzdt$$

The equation becomes:

$$\rho_P r_p\left[(u_z)_P^{t+dt} - (u_z)_P^t\right]\Delta r\Delta z +$$
$$\rho_P r_p(u_r)_p\left[(u_z)_E^{t+dt} - (u_z)_O^{t+dt}\right]\frac{\Delta z\Delta t}{2} +$$
$$\rho_P r_p(u_z)_p\left[(u_z)_N^{t+dt} - (u_z)_S^{t+dt}\right]\frac{\Delta r\ \Delta t}{2} =$$
$$-r_p\left(\frac{\partial p}{\partial z}\right)_P \Delta r\Delta z\Delta t - g_z\rho_P r_p\ \Delta r\ \Delta z\ \Delta t + \quad (31)$$
$$\mu r_P\left[(u_z)_E^{t+dt} - 2(u_z)_P^{t+dt} + (u_z)_O^{t+dt}\right]\frac{\Delta z\Delta t}{\Delta r} +$$
$$\mu\left[(u_z)_E^{t+dt} - (u_z)_O^{t+dt}\right]\frac{\Delta z\ \Delta t}{2} +$$
$$\mu r_p\left[(u_z)_N^{t+dt} - 2(u_z)_P^{t+dt} + (u_z)_S^{t+dt}\right]\frac{\Delta r\Delta t}{\Delta z}$$

The equation can therefore be formulated as follows:

$$A(i,j)(T)_{(i+1,j)}^{k+1} + B(i,j)(T)_{(i-1,j)}^{k+1} + C(i,j)(T)_{(i,j)}^{k+1} +$$
$$E(i,j)(T)_{(i,j+1)}^{k+1} + F(i,j)(T)_{(i,j-1)}^{k+1} = D(i,j)$$

where:

$$A(i,j) = -\mu r_P\frac{\Delta z\ \Delta t}{\Delta r} - \mu\frac{\Delta z\ \Delta t}{2} + r_P\rho_P(u_r)_p\frac{\Delta z\ \Delta t}{2}$$

$$B(i,j) = -\mu r_P\frac{\Delta z\ \Delta t}{\Delta r} + \mu\frac{\Delta z\ \Delta t}{2} - r_P\rho_P(u_r)_p\frac{\Delta z\ \Delta t}{2}$$

$$C(i,j) = \rho_P r_p\Delta r\ \Delta z + 2\mu r_P\frac{\Delta r\ \Delta t}{\Delta z} + 2\mu r_p\frac{\Delta z\ \Delta t}{\Delta r}$$

$$D(i,j) = \rho_P r_p(u_z)_P^t\ \Delta r\Delta z - r_p\left(\frac{\partial p}{\partial z}\right)_P \Delta r\ \Delta z\ \Delta t -$$
$$g_z r_P\rho_P\ \Delta r\ \Delta z\ \Delta t$$

$$E(i,j) = -\mu r_P\frac{\Delta r\ \Delta t}{\Delta z} + r_P\rho_P(u_z)_P\frac{\Delta r\ \Delta t}{2}$$

$$F(i,j) = -\mu r_P\frac{\Delta r\ \Delta t}{\Delta z} - r_P\rho_P(u_z)_P\frac{\Delta r\ \Delta t}{2}$$

- Conservation of energy

For compressible fluids

$$\int_{vc}\int_{dt}\rho C_p\frac{\partial T}{\partial t}\,\mathrm{r}\,dr\,dz\,dt+\int_{vc}\int_{dt}\rho C_p u_r\frac{\partial T}{\partial r}\,\mathrm{r}\,dr\,dz\,dt+$$
$$\int_{vc}\int_{dt}\rho C_p u_z\frac{\partial T}{\partial z}\,\mathrm{r}\,dr\,dz\,dt=\int_{vc}\int_{dt}\rho\dot{q}_g\,\mathrm{r}\,dr\,dz\,dt+$$
$$\int_{vc}\int_{dt}\frac{1}{r}\frac{\partial}{\partial r}\left(kr\frac{\partial T}{\partial r}\right)\mathrm{r}drdzdt+\int_{vc}\int_{dt}\frac{\partial}{\partial z}\left(k\frac{\partial T}{\partial z}\right)\mathrm{r}drdzdt+ \quad (32)$$
$$\int_{vc}\int_{dt}\mathrm{S}\,\mathrm{r}\,dr\,dz\,dt+$$
$$\int_{vc}\int_{dt}\begin{bmatrix}2\mu\left[\left(\frac{\partial u_r}{\partial r}\right)^2+\left(\frac{u_r}{r}\right)^2+\left(\frac{\partial u_z}{\partial z}\right)^2\right]+\\ \mu\left[\left(\frac{\partial u_z}{\partial r}+\frac{\partial u_r}{\partial z}\right)^2\right]-\\ \frac{2}{3}\mu\left(\frac{1}{r}\frac{\partial(ru_r)}{\partial r}+\frac{\partial u_z}{\partial z}\right)^2\end{bmatrix}\mathrm{r}drdzdt$$

The equation becomes:

$$\rho C_p r_p\left[T_P^{t+dt}-T_P^t\right]\Delta r\Delta z+$$
$$\rho C_p r_p(u_r)_p\left[T_E^{t+dt}-T_O^{t+dt}\right]\frac{\Delta z\Delta t}{2}+$$
$$\rho C_p r_p(u_z)_p\left[T_N^{t+dt}-T_S^{t+dt}\right]\frac{\Delta r\Delta t}{2}=\dot{q}_g\rho r_p\Delta r\Delta z\Delta t+$$
$$k\left[T_E^{t+dt}-T_O^{t+dt}\right]\frac{\Delta z\Delta t}{2}+$$
$$kr_P\left[T_E^{t+dt}-2T_P^{t+dt}+T_O^{t+dt}\right]\frac{\Delta z\Delta t}{\Delta r}+$$
$$kr_p\left[T_N^{t+dt}-2T_P^{t+dt}+T_S^{t+dt}\right]\frac{\Delta r\ \Delta t}{\Delta z}+\bar{\mathrm{S}}r_p\Delta r\Delta z\Delta t+ \quad (33)$$
$$\begin{bmatrix}2r_P\mu\left[\left(\frac{\partial u_r}{\partial r}\right)^2+\left(\frac{u_r}{r}\right)^2+\left(\frac{\partial u_z}{\partial z}\right)^2\right]+\\ \mu r_P\left[\left(\frac{\partial u_z}{\partial r}+\frac{\partial u_r}{\partial z}\right)^2\right]-\\ \frac{2}{3}r_P\mu\left(\frac{1}{r}\frac{\partial(ru_r)}{\partial r}+\frac{\partial u_z}{\partial z}\right)^2\end{bmatrix}_p\Delta r\ \Delta z\ \Delta t$$

The equation can therefore be formulated as follows:

$$A(i,j)(T)_{(i+1,j)}^{k+1}+B(i,j)(T)_{(i-1,j)}^{k+1}+C(i,j)(T)_{(i,j)}^{k+1}+$$
$$E(i,j)(T)_{(i,j+1)}^{k+1}+F(i,j)(T)_{(i,j-1)}^{k+1}=D(i,j)$$

where:

$$A(i,j)=C_p r_r\rho(u_r)_p\frac{\Delta z\ \Delta t}{2}-kr_P\frac{\Delta z\ \Delta t}{\Delta r}-k\frac{\Delta z\ \Delta t}{2}$$

$$B(i,j)=-C_p r_r\rho(u_r)_p\frac{\Delta z\ \Delta t}{2}-kr_P\frac{\Delta z\ \Delta t}{\Delta r}+k\frac{\Delta z\ \Delta t}{2}$$

$$C(i,j)=C_p r_r\rho_p\Delta r\ \Delta z+2kr_P\frac{\Delta z\ \Delta t}{\Delta r}+2kr_P\frac{\Delta r\ \Delta t}{\Delta z}$$

$$D(i,j)=C_p\rho r_p T_P^t\ \Delta r\Delta z+\dot{q}_g\rho r_p\Delta r\Delta z\Delta t+\bar{S}\ r_p\Delta r\Delta z\Delta t+$$
$$\begin{bmatrix}2r_P\mu\left[\left(\frac{\partial u_r}{\partial r}\right)^2+\left(\frac{u_r}{r}\right)^2+\left(\frac{\partial u_z}{\partial z}\right)^2\right]+\\ \mu r_P\left[\left(\frac{\partial u_z}{\partial r}+\frac{\partial u_r}{\partial z}\right)^2\right]-\\ \frac{2}{3}r_P\mu\left(\frac{1}{r}\frac{\partial(ru_r)}{\partial r}+\frac{\partial u_z}{\partial z}\right)^2\end{bmatrix}_p\Delta r\Delta z\Delta t$$

$$E(i,j)=C_p r_p\rho(u_z)_p\frac{\Delta r\ \Delta t}{2}-kr_P\frac{\Delta r\ \Delta t}{\Delta z}$$

$$F(i,j)=-C_p r_p\rho(u_z)_p\frac{\Delta r\ \Delta t}{2}-kr_P\frac{\Delta r\ \Delta t}{\Delta z}$$

For incompressible fluids

$$\int_{vc}\int_{dt}\rho C_p\frac{\partial T}{\partial t}\mathrm{r}drdzdt+\int_{vc}\int_{dt}\rho C_p u_r\frac{\partial T}{\partial r}\,\mathrm{r}drdzdt+$$
$$\int_{vc}\int_{dt}\rho C_p u_z\frac{\partial T}{\partial z}\,\mathrm{r}\,dr\,dz\,dt=\int_{vc}\int_{dt}\rho\dot{q}_g\,\mathrm{r}drdzdt+$$
$$\int_{vc}\int_{dt}\mathrm{S}\,\mathrm{r}\,dr\,dz\,dt+\int_{vc}\int_{dt}\frac{1}{r}\frac{\partial}{\partial r}\left(kr\frac{\partial T}{\partial r}\right)\mathrm{r}drdzdt+$$
$$\int_{vc}\int_{dt}\frac{\partial}{\partial z}\left(k\frac{\partial T}{\partial z}\right)\mathrm{r}drdzdt+ \quad (34)$$
$$\int_{vc}\int_{dt}\begin{bmatrix}2\mu\left[\left(\frac{\partial u_r}{\partial r}\right)^2+\left(\frac{u_r}{r}\right)^2+\left(\frac{\partial u_z}{\partial z}\right)^2\right]\\ +\mu\left[\left(\frac{\partial u_z}{\partial r}+\frac{\partial u_r}{\partial z}\right)^2\right]\end{bmatrix}\mathrm{r}\,dr\,dz\,dt$$

The equation becomes:

$$\rho C_p r_p\left[T_P^{t+dt}-T_P^t\right]\Delta r\Delta z+$$
$$\rho C_p r_p(u_r)_p\left[T_E^{t+dt}-T_O^{t+dt}\right]\frac{\Delta z\Delta t}{2}+$$
$$\rho C_p r_p(u_z)_p\left[T_N^{t+dt}-T_S^{t+dt}\right]\frac{\Delta r\ \Delta t}{2}=\dot{q}_g\rho r_p\Delta r\ \Delta z\ \Delta t+$$
$$k\left[T_E^{t+dt}-T_O^{t+dt}\right]\frac{\Delta z\Delta t}{2}+$$
$$kr_P\left[T_E^{t+dt}-2T_P^{t+dt}+T_O^{t+dt}\right]\frac{\Delta z\Delta t}{\Delta r}+$$
$$kr_p\left[T_N^{t+dt}-2T_P^{t+dt}+T_S^{t+dt}\right]\frac{\Delta r\ \Delta t}{\Delta z}+\bar{\mathrm{S}}\,r_p\ \Delta r\ \Delta z\ \Delta t+ \quad (35)$$
$$\begin{bmatrix}2r_P\mu\left[\left(\frac{\partial u_r}{\partial r}\right)^2+\left(\frac{u_r}{r}\right)^2+\left(\frac{\partial u_z}{\partial z}\right)^2\right]+\\ \mu r_P\left[\left(\frac{\partial u_z}{\partial r}+\frac{\partial u_r}{\partial z}\right)^2\right]\end{bmatrix}_p\Delta r\ \Delta z\ \Delta t$$

The equation can therefore be formulated as follows:

$$A(i,j)(T)_{(i+1,j)}^{k+1} + B(i,j)(T)_{(i-1,j)}^{k+1} + C(i,j)(T)_{(i,j)}^{k+1} + E(i,j)(T)_{(i,j+1)}^{k+1} + F(i,j)(T)_{(i,j-1)}^{k+1} = D(i,j)$$

where:

$$A(i,j) = C_p r_r \rho(u_r)_p \frac{\Delta z\ \Delta t}{2} - k r_P \frac{\Delta z\ \Delta t}{\Delta r} - k \frac{\Delta z\ \Delta t}{2}$$

$$B(i,j) = -C_p r_r \rho(u_r)_p \frac{\Delta z\ \Delta t}{2} - k r_P \frac{\Delta z\ \Delta t}{\Delta r} + k \frac{\Delta z\ \Delta t}{2}$$

$$C(i,j) = C_p r_r \rho_p \Delta r\ \Delta z + 2k r_P \frac{\Delta z\ \Delta t}{\Delta r} + 2k r_P \frac{\Delta r\ \Delta t}{\Delta z}$$

$$D(i,j) = C_p \rho r_p T_P^t\ \Delta r\ \Delta z + \dot{q}_g \rho r_p \Delta r\ \Delta z\ \Delta t + \left[\begin{array}{l} 2r_P \mu \left[\left(\frac{\partial u_r}{\partial r} \right)^2 + \left(\frac{u_r}{r} \right)^2 + \left(\frac{\partial u_z}{\partial z} \right)^2 \right] + \\ \mu r_P \left[\left(\frac{\partial u_z}{\partial r} + \frac{\partial u_r}{\partial z} \right)^2 \right] \end{array} \right]_p \Delta r \Delta z \Delta t + \bar{S}\ \mathrm{r}_P\ \Delta r\ \Delta z\ \Delta t$$

$$E(i,j) = C_p r_p \rho(u_z)_p \frac{\Delta r\ \Delta t}{2} - k r_P \frac{\Delta r\ \Delta t}{\Delta z}$$

$$F(i,j) = -C_p r_p \rho(u_z)_p \frac{\Delta r\ \Delta t}{2} - k r_P \frac{\Delta r\ \Delta t}{\Delta z}$$

Resolution by the Gauss Seidel method:

The algebraic equations previously obtained can be written in the following common form:

$$A(i,j)(\Psi)_{(i+1,j)}^{k+1} + B(i,j)(\Psi)_{(i-1,j)}^{k+1} + C(i,j)(\Psi)_{(i,j)}^{k+1} + E(i,j)(\Psi)_{(i,j+1)}^{k+1} + F(i,j)(\Psi)_{(i,j-1)}^{k+1} = D(i,j)$$

The solution of this equation by the Gauss Seidel method is given by the following form:

$$(\Psi)_{(i,j)}^{k+1} = \frac{D(i,j) - \left[\begin{array}{l} A(i,j)(\Psi)_{(i+1,j)}^{k+1} + B(i,j)(\Psi)_{(i-1,j)}^{k+1} + \\ E(i,j)(\Psi)_{(i,j+1)}^{k+1} + F(i,j)(\Psi)_{(i,j-1)}^{k+1} \end{array} \right]}{C(i,j)}$$

5.2. Degradation kinetics

The set of differential equations 15-21 is solved using the second-order Runge-Kutta method, which can be expressed in the following form:

$$\begin{cases} y_{n+1}^* = y_n + h\ .\ f(x_n, y_n) \\ y_{n+1} = y_n + \frac{h}{2} \left[f(x_n, y_n) + f(x_{n+1}, y_{n+1}^*) \right] \\ y_0\ \textit{initial condition} \end{cases}$$

6. RESULTS AND DISCUSSION

The numerical systems obtained in the previous paragraphs have been written and solved numerically in Fortran language. The results of the simulation, based on the parameters given in the tables 1 and 2, are given in figures 3 to 11.

Table 1. Parameters used in the fluid dynamics model

Parameter	Value
Dimensions of the digester (m)	Height = 15 Radius = 5
Density of the fluid (kg/m^3)	1006
Velocity of the fluid (m/s)	1,4.10^{-5}
Dynamic viscosity (Pa. s)	0,7.10^{-3}
Temperature (K)	310

Table 2. Parameters used in the biogas production model [29]

Parameter	Value		
The three degradation kinetic constants (Day^{-1})	0.31	0.29	0.27
Acidogenic biomass (kg/kg)	0.16		
Methanogenic biomass (kg/kg)	0.011		
Rate constant for the death of acidogenic biomass (Day-^{1})	0.4		
Rate constant for the death of methanogenic biomass (Day-^{1})	0.05		
Methane efficiency ratio	0.6		
Acetate efficiency ratio	0.9		

Results:

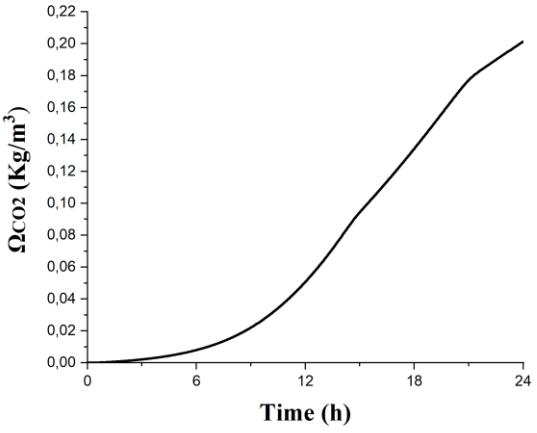

Fig. 3. Profile of cumulative production of Carbon dioxide as a function of time.

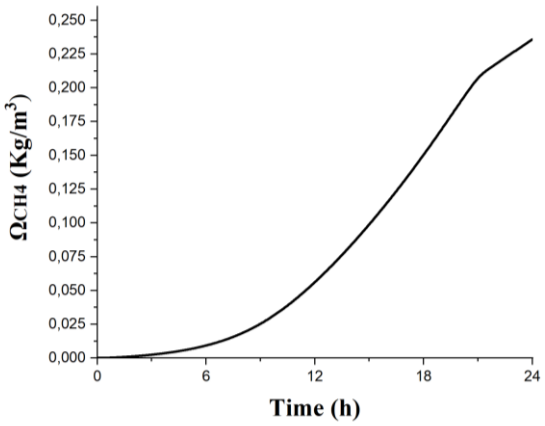

Fig. 4. Profile of cumulative production of methane as a function of time.

The plot of figure 3 und 4 indicate that the accumulations of CH_4 and CO_2 productions increase with time. This increase is due to the continuous production of these two gases over time.

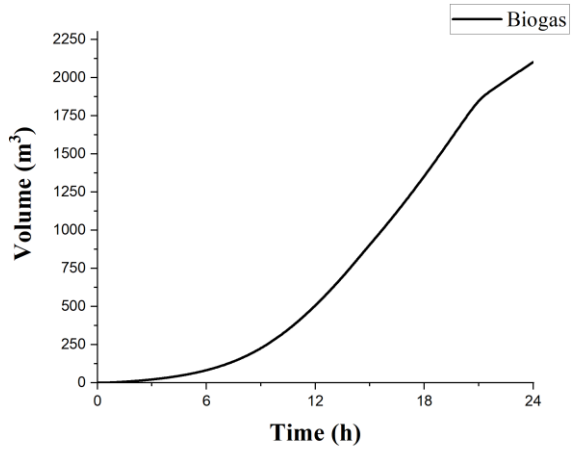

Fig. 5. Evolution of biogas production as a function of time.

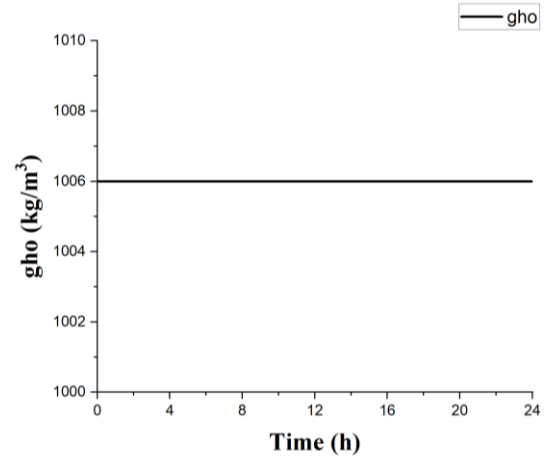

Fig. 6. The density as a function of time (in the compressible case).

The biogas production is shown as a function of time in Figure 5. Biogas is mainly composed of CH_4 and CO_2 and its production is proportional to the production of these two gases. The plot of this figure shows that biogas production begins around 3h and starts to be very important after 6h. Note that from this moment, the rate of production of methane and carbon dioxide becomes very fast (figures 3 and 4).

Figure (6) shows the density as a function of time. The plot in this figure shows that the density is almost constant during anaerobic digestion. This can be explained by the fact that the amount of biogas produced at a specific time is negligible compared to the amount of effluent in the digester.

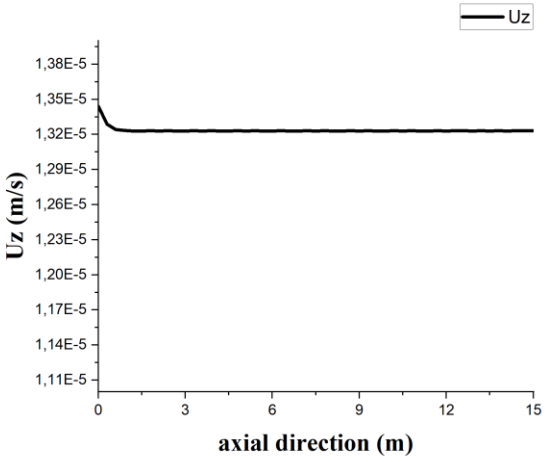

Fig. 7. velocity profile in the axial direction (in the compressible case).

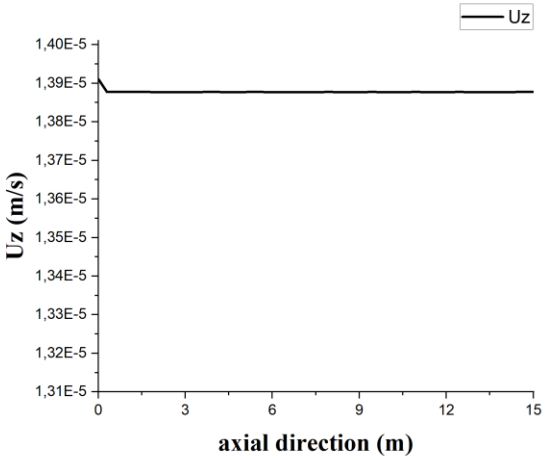

Fig. 8. velocity profile in the axial direction (in the incompressible case)

Successively, figures (7) and (8) illustrate the evolution of the velocity profile in the axial direction in the compressible and incompressible cases. In both figures, the axial velocity decreases at the inlet of the digester. This is due to the change in cross-sectional area between the fluid

inlet tubes and the digester and also to the effect of the weight of the fluid. In both cases studied, it can be seen that the axial velocity stabilises around a mean value, more rapidly in the incompressible case. We also note that the velocity is almost the same because the difference between the average velocities in the two cases is negligible, at around 6.10^{-7}.

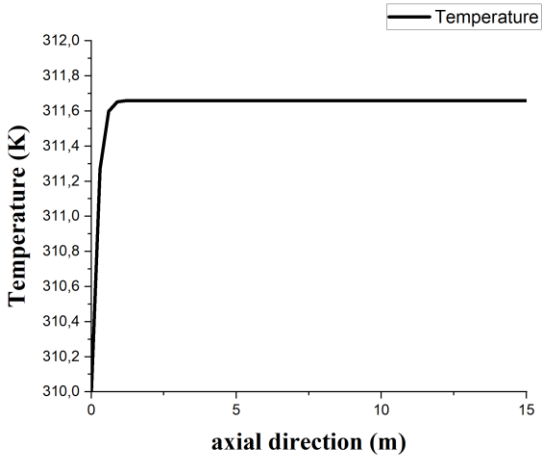

Fig. 9. Profile of the temperature in the axial direction (in the compressible case)

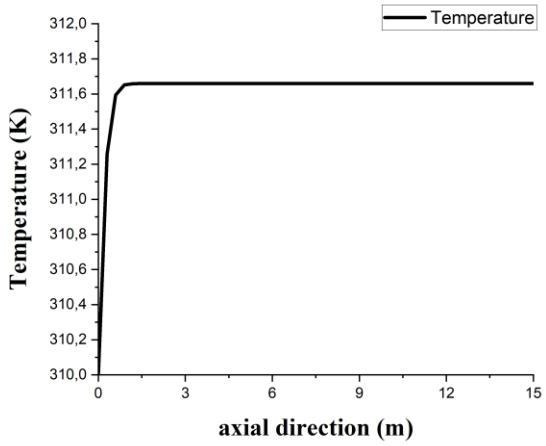

Fig. 10. Profile of the temperature in the axial direction (in the incompressible case).

Figures (9) and (10) illustrate the evolution of the temperature profile along the axial direction of the digester in the compressible and incompressible cases. The plots of the two figures are identical. They indicate that the effluent temperature increases slightly with altitude in the first metre following the height of the digester and stabilises thereafter. This result can be explained by the temperature exchange between the influent and the fluid already present in the digester. The latter gains in temperature from the energy released by the exothermic chemical reactions that take place during anaerobic digestion.

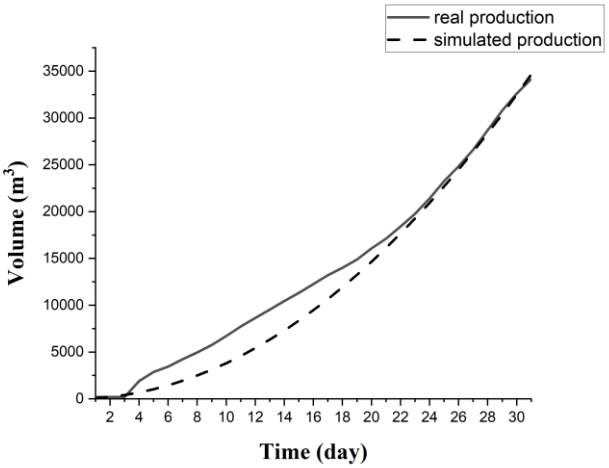

Fig. 11. Cumulative production of biogas as a function of time

Figure 11 shows the cumulative biogas production over 30 days for the real and simulated cases. The plots in these figures indicate that the accumulations of biogas production increase over time. From day 1 to day 22, the differences in biogas production rates (actual and simulated) are due to the instability of the amount of dissolved carbon in the pulp and paper mill effluent, which differs from day to another. Furthermore, after day 23, the simulation results for biogas production are in agreement with the experimental results.

7. CONCLUSION

The present study was carried out to compare and examine the evolution of physical and biological quantities of the anaerobic digestion phenomenon in the digester, in the compressible and incompressible cases. The aim was to gain a better understanding of fluid dynamics in the digester over time, to understand the impact of biogas production on fluid characteristics and to improve biogas production. The results showed that inside the digester, between the two cases studied, variations in density and velocity were relatively negligible, while temperature was unaffected. According to the simulation results, the amount of biogas produced during the process has no influence on the fluid characteristics. In conclusion, it is more practical to model the phenomenon on the assumption that the fluid is incompressible, because on the one hand this simplifies the calculations, and on the other hand it guarantees the convergence of the solution and therefore the stability of our numerical code. In addition, the progression of real biogas production as a function of time shows that mixing improves the kinetics of degradation and production during the anaerobic digestion of paper factory effluents. This means that mixing is essential to maximise the efficiency of anaerobic digestion and to obtain optimum performance from the process. In fact, this is consistent with various results in the literature [40, 41]. But the benefits don't stop

there. The pulp and paper industry and similar businesses benefit not only from a valuable renewable energy source, but also from reduced waste and greenhouse gas emissions. Finally, we propose to study the effects of turbulence on the production and quality of the biogas produced.

REFERENCES

[1] Kokko, M.; Koskue, V.; et Rintala, J. 2018. Anaerobic digestion of 30−100-year-old boreal lake sedimented fibre from the pulp industry: Extrapolating methane production potential to a practical scale. *Water Research 133* : 218-226.

[2] Virkutyte, J. 2017. Aerobic Treatment of Effluents From Pulp and Paper Industries. Elsevier. In *Current Developments in Biotechnology and Bioengineering* : 103-130.

[3] Kumar, A.; et Ramanathan, A. 2021. Design of an agitator in the anaerobic digester for mixing of biomass slurry. *Materials Today: Proceedings 46* : 9678-9682.

[4] Chatterjee, P.; Lahtinen, L.; Kokko, M.; et Rintala, J. 2018. Remediation of sedimented fiber originating from pulp and paper industry: Laboratory scale anaerobic reactor studies and ideas of scaling up. Water Research 143 : 209-217.

[5] Show, K.-Y.; et Lee, D.-J. 2017. Anaerobic Treatment Versus Aerobic Treatment. Elsevier. In *Current Developments in Biotechnology and Bioengineering* : 205-230.

[6] Simate, G. S.; Cluett, J.; Iyuke, S. E.; Musapatika, E. T.; Ndlovu, S.; Walubita, L. F.; et Alvarez, A. E. 2011. The treatment of brewery wastewater for reuse: State of the art. *Desalination 273* (2-3) : 235-247.

[7] Ashrafi, O.; Yerushalmi, L.; et Haghighat, F. 2015. Wastewater treatment in the pulp-and-paper industry: A review of treatment processes and the associated greenhouse gas emission. *Journal of Environmental Management 158* : 146-157.

[8] Qi, W.-K.; Liu, L.-F.; Shi, Q.; Wang, C.; Li, Y.-Y.; et Peng, Y. 2021. Detailed composition evolution of food waste in an intermittent self-agitation anaerobic digestion baffled reactor. *Bioresource Technology 320* : 124342.

[9] Intanin, J.; Hussaro, K.; et Teekasap, S. 2018. Lab-scale anaerobic co-digestion of manure with wastewater from toddy palm process for increased biogas production. *GMSARN International Journal 12* : 56-64.

[10] Chan, Y. J.; Chong, M. F.; Law, C. L.; et Hassell, D. G. 2009. A review on anaerobic–aerobic treatment of industrial and municipal wastewater. *Chemical Engineering Journal 155* (1-2) : 1-18.

[11] Gozde Ozbayram, E. 2021. Waste to energy: valorization of spent tea waste by anaerobic digestion. *Environmental Technology 42* (22) : 3554-3560.

[12] Cruz, I. A.; Andrade, L. R. S.; Bharagava, R. N.; Nadda, A. K.; Bilal, M.; Figueiredo, R. T.; et Ferreira, L. F. R. 2021. An overview of process monitoring for anaerobic digestion. *Biosystems Engineering 207* : 106-119.

[13] Leonzio, G. 2019. Fluid dynamic study of anaerobic digester: optimization of mixing and geometric configuration by using response surface methodology and factorial design. *Renewable Energy 136* : 769-780.

[14] Ambaye, T. G.; Rene, E. R.; Dupont, C.; Wongrod, S.; et van Hullebusch, E. D. 2020. Anaerobic Digestion of Fruit Waste Mixed With Sewage Sludge Digestate Biochar: Influence on Biomethane Production. *Frontiers in Energy Research 8* : 31.

[15] HUSSARO, K. 2022. Effects of Oil Palm Shell Biochar to Tuna Wastewater on Biogas Production and Methane Yield by Anaerobic Sequencing Batch Reactor (ASBR): Mesophilic Condition. *GMSARN International Journal 16* : 331-338.

[16] Martínez, M.; Martínez, M.; Fajardo, M.; et López, J. 2011. Modeling flow inside an anaerobic digester by CFD techniques. *International Journal of Energy and Environment 2* (6) : 963-974.

[17] Kigozi, R.; Aboyade, A.; et MUZENDA, E. 2014. Biogas Production Using the Organic Fraction of Municipal Solid Waste as Feedstock. *International Journal of Research in Chemical, Metallurgical and Civil Engineering (IJRCMCE) 1*.

[18] N. Boontian. 2014. *Conditions Of The Anaerobic Digestion Of Biomass*. https://zenodo.org/record/1096285

[19] Tian, L.; Shen, F.; Yuan, H.; Zou, D.; Liu, Y.; Zhu, B.; et Li, X. 2014. Reducing agitation energy-consumption by improving rheological properties of corn stover substrate in anaerobic digestion. *Bioresource Technology 168* : 86-91.

[20] Jimenez, J.; Latrille, E.; Harmand, J.; Robles, A.; Ferrer, J.; Gaida, D.; Wolf, C.; Mairet, F.; Bernard, O.; Alcaraz-Gonzalez, V.; Mendez-Acosta, H.; Zitomer, D.; Totzke, D.; Spanjers, H.; Jacobi, F.; Guwy, A.; Dinsdale, R.; Premier, G.; Mazhegrane, S.; … Steyer, J.-P. 2015. Instrumentation and control of anaerobic digestion processes: a review and some research challenges. *Reviews in Environmental Science and Bio/Technology 14* (4): 615-648.

[21] Draa, K. C.; Zemouche, A.; Alma, M.; Voos, H.; et Darouach, M. 2019. Control of Anaerobic Digestion Process. Elsevier. In *New Trends in Observer-based Control* : 99-135.

[22] Uçkun Kiran, E.; Stamatelatou, K.; Antonopoulou, G.; et Lyberatos, G. 2016. Production of biogas via anaerobic digestion. Elsevier. In *Handbook of Biofuels Production* : 259-301.

[23] Azargoshasb, H.; Mousavi, S. M.; Amani, T.; Jafari, A.; et Nosrati, M. 2015. Three-phase CFD simulation coupled with population balance equations of anaerobic syntrophic acidogenesis and methanogenesis reactions in a continuous stirred bioreactor. *Journal of Industrial and Engineering Chemistry 27* : 207-217.

[24] Oates, A.; Neuner, T.; Meister, M.; Borman, D.; Camargo-Valero, M.; Sleigh, A.; et Fischer, P. 2020. Modelling Mechanically Induced Non-Newtonian Flows to Improve the Energy Efficiency of Anaerobic Digesters. *Water 12* (11) : 2995.

[25] El-Fadel, M.; Findikakis, A. N.; et Leckie, J. O. 1996. Numerical Modelling of Generation and Transport of Gas and Heat in Landfills I. Model Formulation. *Waste Management & Research: The Journal for a Sustainable Circular Economy 14* (5) : 483-504.

[26] Vavilin, V. A.; Rytov, S. V.; Lokshina, L. Ya.; Pavlostathis, S. G.; et Barlaz, M. A. 2003. Distributed model of solid waste anaerobic digestion: Effects of leachate recirculation and pH adjustment. *Biotechnology and Bioengineering 81* (1) : 66-73.

[27] Men-La-Yakhaf, S.; Gueraoui, K.; et Driouich, M. 2014. New numerical and mathematical code reactive mass transfer and heat storage facilities of argan waste. *Advanced Studies in Theoretical Physics 8* : 485-498.

[28] Pinto, A. M. F. R.; Oliveira, V. B.; et Falcão, D. S. 2018. Status and research trends of direct alcohol fuel cell technology. Elsevier. In *Direct Alcohol Fuel Cells for Portable Applications* : 307-329.

[29] Laabyech, A.; Men-la-yakhaf, S.; Kifani-Sahban, F.; Gueraoui, K.; et Wahby, I. 2018. Mathematical and Numerical Simulation for the Production of Biogas from Liquid Effluent of Paper Pulp Mill. *International Journal on Energy Conversion (IRECON) 6* (4) : 129.

[30] Pariente, M. I.; Segura, Y.; Molina, R.; et Martínez, F. 2020. Wastewater treatment as a process and a resource. Elsevier. In *Wastewater Treatment Residues as Resources for Biorefinery Products and Biofuels* : 19-45.

[31] Gerba, C. P.; et Pepper, I. L. 2015. Municipal Wastewater Treatment. Elsevier. In *Environmental Microbiology* : 583-606.

[32] Wang, L. K., Hung, Y.-T., & Shammas, N. K. (Éds.). 2005. *Physicochemical treatment processes*. Humana Press.

[33] Nguyen, D.; Nitayavardhana, S.; Sawatdeenarunat, C.; Surendra, K. C.; et Khanal, S. K. 2019. Biogas Production by Anaerobic Digestion: Status and Perspectives. Elsevier. In *Biofuels: Alternative Feedstocks and Conversion Processes for the Production of Liquid and Gaseous Biofuels* : 763-778.

[34] Li, D.; Liu, S.; Mi, L.; Li, Z.; Yuan, Y.; Yan, Z.; et Liu, X. 2015. Effects of feedstock ratio and organic loading rate on the anaerobic mesophilic co-digestion of rice straw and pig manure. *Bioresource Technology 187* : 120-127.

[35] Laabyech, A.; Men-la-yakhaf, S.; Kifani-Sahban, F.; Gueraoui, K.; et Wahby, I. 2018. Effects of the Variation of Organic Carbon Rate on the Biogas Production During Anaerobic Digestion. *International Review of Mechanical Engineering (IREME) 12* (10) : 854.

[36] Monod, J. 1949. THE GROWTH OF BACTERIAL CULTURES. *Annual Review of Microbiology 3* (1) : 371-394.

[37] Katopodes, N. D. 2019. Finite-Element and Finite-Volume Methods for Scalar Transport. Elsevier. In *Free-Surface Flow* : 198-258.

[38] McClarren, R. G. 2018. Iterative Methods for Linear Systems. Elsevier. In *Computational Nuclear Engineering and Radiological Science Using Python* : 145-172.

[39] Sonar, T. 2016. Classical Finite Volume Methods. Elsevier. In *Handbook of Numerical Analysis* Vol. 17, : 55-76.

[40] Coutu, A.; Mottelet, S.; Guérin, S.; Rocher, V.; Pauss, A.; et Ribeiro, T. 2022. Methane yield optimization using mix response design and bootstrapping: application to solid-state anaerobic co-digestion process of cattle manure and damp grass. *Bioresource Technology Reports 17* : 100883.

[41] Arelli, V.; Mamindlapelli, N. K.; Begum, S.; Juntupally, S.; et Anupoju, G. R. 2021. Solid state anaerobic digestion of food waste and sewage sludge: Impact of mixing ratios and temperature on microbial diversity, reactor stability and methane yield. *Science of The Total Environment 793* : 148586.

NOMENCLATURES

Ω_i	Organic carbon (kg/m^3)
Ω_{aq}	Aqueous organic carbon (kg/m^3)
Ω_{Ba}	Acidogenic biomass carbon (kg/m^3)
Ω_{Bm}	Methanogenic biomass carbon (kg/m^3)
Ω_{Ac}	Acetate carbon (kg/m^3)
Ω_{CH_4}	Methane carbon (kg/m^3)
Ω_{CO_2}	Dioxide carbon (kg/m^3)
h_i	degradation kinetic constants.
Y_A	the ratio of the mass of acidogenic biomass produced to the mass of carbon used (kg/kg)
Y_M	the ratio of the mass of methanogenic biomass produced to the mass of acetate used (kg/kg)
D_A	Constant of the mortality rate of the acidogenic biomass (day^{-1})
D_M	Constant of the mortality rate of the methanogenic biomass (day^{-1})
H_{Sa}	Half saturation constant of the acidogenic biomass (kg/m^3)
H_{Sm}	Half saturation constant of the methanogenic biomass (kg/m^3)
Y_{CH_4}	Methane efficiency ratio (kg/kg)
Y_{AC}	Acetate efficiency ratio (kg/kg)
ρ	Density of the fluid (kg/m3)
u	Velocity of the fluid (m/s)
μ	Dynamic viscosity (Pa. s)
λ_a	Maximum growth rate constant of the acidogenic biomass (day^{-1})
λ_m	Maximum growth rate constant of the methanogenic biomass (day^{-1})